

Fly0: Decoupling Semantic Grounding from Geometric Planning for Zero-Shot Aerial Navigation

Zhenxing Xu ^{*1} Brikit Lu ^{*2} Weidong Bao ¹ Zhengqiu Zhu ³ Junsong Zhang ¹ Hui Yan ⁴ Wenhao Lu ³
 Ji Wang ¹

Abstract

Current Visual-Language Navigation (VLN) methodologies face a trade-off between semantic understanding and control precision. While Multimodal Large Language Models (MLLMs) offer superior reasoning, deploying them as low-level controllers leads to high latency, trajectory oscillations, and poor generalization due to weak geometric grounding. To address these limitations, we propose Fly0, a framework that decouples semantic reasoning from geometric planning. The proposed method operates through a three-stage pipeline: (1) an MLLM-driven module for grounding natural language instructions into 2D pixel coordinates; (2) a geometric projection module that utilizes depth data to localize targets in 3D space; and (3) a geometric planner that generates collision-free trajectories. This mechanism enables robust navigation even when visual contact is lost. By eliminating the need for continuous inference, Fly0 reduces computational overhead and improves system stability. Extensive experiments in simulation and real-world environments demonstrate that Fly0 outperforms state-of-the-art baselines, improving the Success Rate by over 20% and reducing Navigation Error (NE) by approximately 50% in unstructured environments. Our code is available at <https://github.com/xuzhenxing1/Fly0>.

1. Introduction

VLN represents a pivotal challenge in embodied AI, integrating computer vision, natural language processing, and robotics. The goal is to endow autonomous agents, partic-

ularly UAVs, with the ability to interpret natural language instructions and navigate complex 3D environments to reach specific targets (Liu et al., 2023). Unlike traditional point-to-point navigation, VLN requires the agent to perform fine-grained cross-modal alignment, grounding linguistic concepts (e.g., “the blue tent behind the tree”) into physical spatial representations.

Existing VLN methodologies, however, grapple with the tension between semantic understanding and control precision. Early works primarily adopted end-to-end architectures (Sautenkov et al., 2025; Wang et al., 2025; 2024; Gao et al., 2025; Liu et al., 2023), learning a direct mapping from raw sensory inputs to control commands. While pioneering, these “black-box” models often lack interpretability and struggle to generalize to unseen environments due to weak semantic grounding.

To address these limitations, recent research has pivoted toward MLLMs acting as zero-shot agents (Zhang et al., 2025; Zhao et al., 2025; Xu et al., 2025; Liu et al., 2024; Hu et al., 2025). By reformulating navigation as a Visual Question Answering (VQA) or text-generation task, these methods leverage the vast world knowledge of MLLMs to generate discrete actions (e.g., “turn left”). While promising, we identify a critical paradigm misalignment in current state-of-the-art MLLM-based agents: they conflate semantic reasoning with motion execution.

Specifically, forcing an MLLM to function as a low-level controller introduces three formidable challenges:

Granularity Mismatch: Linguistic instructions are inherently sparse and semantic, whereas UAV control requires dense, continuous, and geometric signals. Mapping language directly to discrete movement steps (e.g., “move forward 1m”) often results in jerky, suboptimal trajectories that fail to align with the smoothness of physical motion.

High Inference Latency: The auto-regressive nature of MLLMs incurs high computational costs. Relying on them for high-frequency decision-making introduces significant latency, which is detrimental to the safety and efficiency of real-time UAV navigation.

¹National Key Laboratory of Big Data and Decision, National University of Defense Technology ²Phytium Technology ³State Key Laboratory of Digital Intelligent Modeling and Simulation, National University of Defense Technology ⁴Information Support Force Engineering University. Correspondence to: Weidong Bao <wdbao@nudt.edu.cn>.

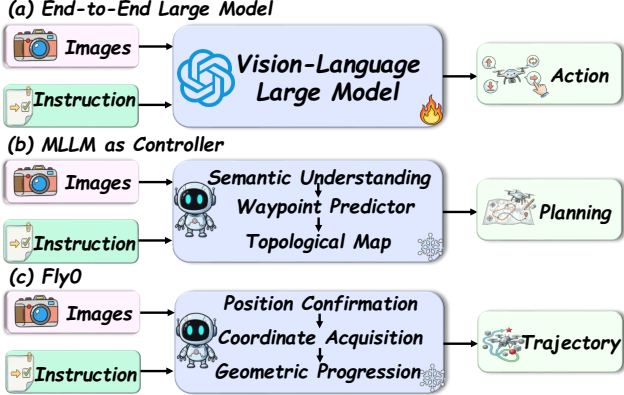


Figure 1. Illustration of three navigation architectures. (a) End-to-End models directly output actions. (b) Methods using MLLM as a controller typically rely on waypoint prediction and topological maps. (c) Our proposed **Fly0** framework leverages the semantic reasoning of MLLMs for precise *Coordinate Acquisition* and *Geometric Progression*, enabling the generation of smooth metric trajectories in a zero-shot manner.

Fragile Context Maintenance: Continuous viewpoint changes during flight can introduce visual distractors or temporary occlusions. When the MLLM is responsible for frame-by-frame control, these visual perturbations can easily disrupt its reasoning chain, leading to navigation failure.

We attribute the high latency and control instability observed in existing methods to a fundamental paradigm misalignment. These approaches compel MLLMs to handle fine-grained and high-frequency motion control, a task for which they are ill-suited, rather than leveraging their superior semantic reasoning capabilities. We posit that the primary bottleneck in VLN is “Semantic Grounding” rather than low-level action generation. Consequently, we introduce Fly0 (Figure 1), a novel modular framework that decouples the VLN task into two complementary stages:

(1) MLLM-based Explicit Semantic Mapping: In this stage, the MLLM is tasked exclusively with grounding instructions to 2D pixel coordinates within the RGB view. This design circumvents the computational complexity of direct action generation and extensive textual reasoning. As a result, it significantly reduces inference latency.

(2) Geometry-Aware Robust Planning: We project the identified 2D targets into a 3D world coordinate system utilizing depth information and camera intrinsics. Deriving explicit destination coordinates effectively mitigates MLLM hallucinations often triggered by target loss. Subsequently, we leverage real-time LiDAR point clouds and the Ego-Planner algorithm to generate optimal and collision-free trajectories. This architecture effectively harmonizes the high-level semantic understanding of LLMs with the rigorous safety and real-time guarantees required for low-level navigation.

Our main contributions are summarized as follows:

- ❶ **Paradigm Shift in VLN Control:** We propose Fly0, which redefines the MLLM’s role from a direct controller to a dedicated *Semantic Reasoning Engine*. This decoupling effectively resolves the conflict between the slow, high-level reasoning of LLMs and the fast, low-level requirements of flight control.
- ❷ **Interpretable Cross-Modal Pipeline:** We construct a robust pipeline that explicitly bridges “Language-Vision” semantics with “3D Geometric” space. By integrating 2D LLM grounding with depth-guided 3D back-projection, we achieve a system that is both semantically intelligent and geometrically precise.
- ❸ **Superior Generalization and Performance:** Extensive experiments demonstrate that Fly0 significantly outperforms existing state-of-the-art methods. We observe substantial improvements in key metrics, specifically Success Rate (SR) and Navigation Error (NE). These results empirically validate the effectiveness of decoupling semantic mapping from control execution. Notably, the system maintains a high navigation success rate during physical deployment in our custom real-world environment, highlighting its robust generalization capabilities.

2. Related Work

2.1. End-to-End Vision-Language Navigation

Early research in VLN predominantly adopted end-to-end learning paradigms. Pioneering works (Anderson et al., 2018; Fried et al., 2018) modeled VLN as a sequence-to-sequence problem, employing RNNs to map visual features and language embeddings directly into low-level actions. Subsequent studies introduced Transformer-based architectures (Hao et al., 2020; Hong et al., 2021) and reinforcement learning strategies (Wang et al., 2019) to enhance long-horizon dependency modeling and cross-modal alignment. More recently, the rapid advancement of MLLMs has significantly improved visual-linguistic capabilities, prompting numerous approaches to fine-tune these pre-trained models as powerful (Sautenkov et al., 2025; Wang et al., 2025; 2024; Gao et al., 2025; Liu et al., 2023).

Despite achieving impressive performance on specific benchmarks, these methods suffer from an inherent “black box” nature, lacking both interpretability and robust semantic grounding. They tend to memorize dataset-specific trajectories rather than acquiring generalizable spatial reasoning, which leads to significant performance degradation in unseen environments (Zhu et al., 2020). Furthermore, the entanglement of visual perception, language understanding, and motion control within a single monolithic network complicates fault diagnosis and restricts adaptation to the agile kinematics of UAVs.

2.2. MLLM-based Navigation Agents

The emergence of MLLMs has shifted the paradigm towards zero-shot or few-shot navigation agents (Zhou et al., 2024; Huang et al., 2022). These methods leverage the extensive world knowledge and reasoning capabilities of models like GPT-4V or LLaVA to interpret complex instructions. Typically, these frameworks formulate navigation as a VQA or text-generation task, where the model iteratively observes the environment and outputs discrete action descriptions (e.g., “turn left 30 degrees”) (Liang et al., 2022; Shah et al., 2023). While these agents demonstrate superior semantic understanding compared to end-to-end models (Zhang et al., 2025; Zhao et al., 2025; Xu et al., 2025; Liu et al., 2024; Hu et al., 2025), they suffer from a critical granularity mismatch. By forcing MLLMs to function as low-level motion controllers, these methods expose the model to high-frequency decision-making loops for which they are ill-suited. This results in high inference latency and trajectory oscillations, as MLLMs lack the inherent geometric intuition required for precise continuous control. Unlike these approaches, our proposed Fly0 decouples the reasoning process from execution, employing the MLLM strictly for semantic grounding while offloading control to a specialized geometric planner.

2.3. Modular and Map-based Navigation

To mitigate the limitations of end-to-end learning, modular approaches decompose VLN into explicit sub-tasks: mapping, localization, and planning. Several works construct topological graphs (Chen et al., 2021) or metric semantic maps (Georgakis et al., 2022) to anchor instructions in a persistent spatial memory. However, constructing global semantic maps is computationally expensive and sensitive to state estimation errors, particularly in drone-based navigation where viewpoints change rapidly. Our approach differs from these heavy mapping frameworks by adopting a lightweight, “perceive-and-act” strategy. Instead of maintaining a global semantic map, Fly0 performs real-time explicit semantic grounding on 2D views and projects these signals into 3D space immediately for local planning. This design combines the semantic richness of MLLMs with the robustness of geometric planning without the overhead of maintaining a complex global representation.

3. Problem Formulation

Given a natural language instruction L and egocentric visual observations V , the objective of the UAV is to plan a sequence of actions within a continuous 3D space to reach a designated target location \mathbf{x}_{goal} . At each time step t , the agent employs a policy π to predict the subsequent action a_t based on the current visual input v_t and the instruction L . The positional update of the UAV is governed by its kinematic model (or state transition function) \mathcal{T} , formally

expressed as:

$$\mathbf{x}_t = \mathcal{T}(\mathbf{x}_{t-1}, \pi(v_t, L)). \quad (1)$$

Upon completion of the trajectory, the navigation task is considered successful if the Euclidean distance between the final position and the target \mathbf{x}_{goal} falls within a predefined threshold δ . Accordingly, the Success Rate (\mathcal{S}_{rate}) is defined as the probability of satisfying this distance constraint:

$$\mathcal{S}_{rate} = \mathbb{P}(\|\mathcal{T}(\pi(\mathbf{x}_0, V, L)) - \mathbf{x}_{goal}\| < \delta), \quad (2)$$

where $\|\cdot\|$ denotes the L_2 norm. Consequently, the core objective of Aerial VLN is to identify an optimal policy π^* that maximizes the task success rate:

$$\pi^* = \arg \max_{\pi} \mathcal{S}_{rate}. \quad (3)$$

Diverging from conventional methods that attempt to learn π^* directly, our approach reformulates the problem. Instead of end-to-end policy optimization, our primary objective is to utilize L and V to estimate the 3D world coordinates of the destination, denoted as G_{world} . Subsequently, we employ Ego-Planner to generate real-time, collision-free trajectories, thereby accomplishing the visual-language navigation task.

4. Methodology: The Fly0 Framework

In this section, we present the Fly0 framework, a modular and robust architecture designed for zero-shot UAV-VLN. As illustrated in Figure 2, our core philosophy addresses the “semantic-geometric gap” inherent in aerial navigation by decoupling the problem into two synergistic phases: *High-Level Semantic Goal Grounding* and *Low-Level Explicit Path Planning*.

Unlike end-to-end methods that map pixels directly to actions, Fly0 employs a hierarchical strategy to address sample inefficiency and lack of interpretability. The framework aligns natural language instructions with visual observations to identify a 2D destination. To enable physical execution, we introduce a depth-informed back-projection that recovers the 3D coordinates of the target. This explicit localization grants the system object permanence, allowing the UAV to navigate when visual contact is lost due to occlusion, maneuvering, or field-of-view constraints. Finally, the Ego-Planner utilizes real-time LiDAR data to generate optimal, collision-free trajectories in cluttered environments.

4.1. MLLM-based 2D Semantic Goal Grounding

The perception frontend of our framework is powered by a MLLM, denoted as Φ_{VLM} . This module functions as the semantic reasoning engine, responsible for parsing user intent and grounding it within the visual scene. Formally, at each discrete time step t , the agent captures an ego-centric RGB image $I_t \in \mathbb{R}^{H \times W \times 3}$. The system receives a natural

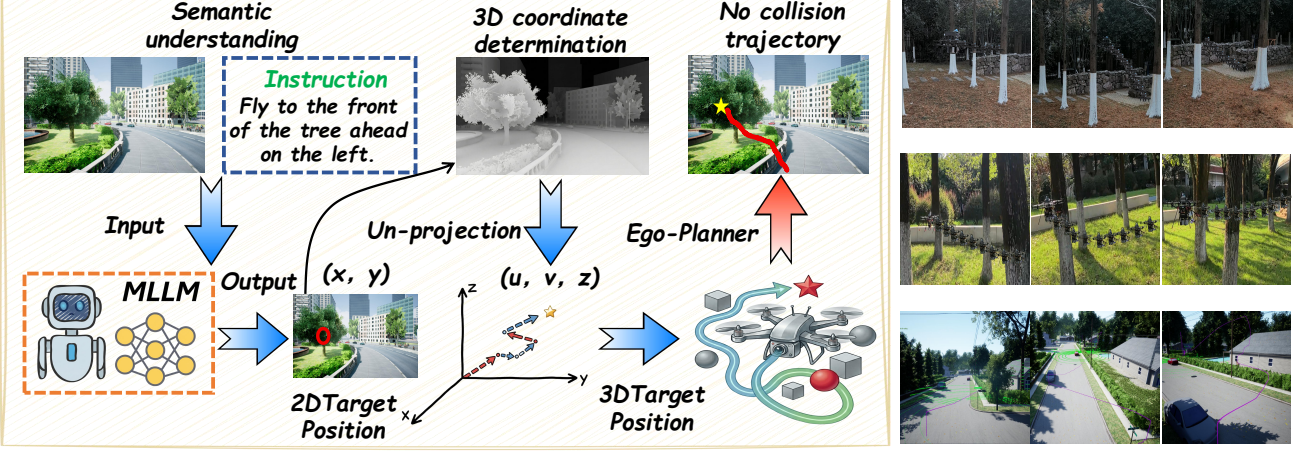


Figure 2. Schematic diagram of the proposed visual-language navigation system. The framework leverages an MLLM to bridge the gap between semantic instructions and metric navigation. By grounding the user’s command into a 2D target position, the system employs an un-projection module to derive the corresponding spatial coordinates. This precise 3D localization enables the Ego-Planner (Zhou et al., 2020) to compute optimal, obstacle-avoiding paths, as demonstrated in the field tests shown on the right.

language instruction L , which may contain abstract spatial descriptions or object attributes. The goal of Φ_{VLM} is to perform Referring Coordinate Grounding, mapping the linguistic query to a specific pixel location. To maximize the reasoning capability of the MLLM, we design a prompt engineering strategy (detailed in Appendix A). The prompt guides Φ_{VLM} to first analyze the global scene context, then identify candidate objects matching the description in L , and finally select the most probable target. The model output is constrained to a structured JSON format, predicting the 2D target coordinates $\mathbf{p}_{2D} = (x, y)$, where $x \in [0, W]$ and $y \in [0, H]$. This structured output ensures that the downstream geometric modules receive a standardized input, isolating the semantic ambiguity within the VLM layer. To mitigate the depth estimation uncertainty inherent in long-range sensing, we implement a low-frequency re-grounding strategy (e.g., at 0.5 Hz). By querying the MLLM every two seconds, the system progressively refines the destination coordinates as the UAV approaches the target. This mechanism effectively corrects initial projection errors caused by the sensor’s degradation at distance, ensuring precise terminal navigation.

4.2. From 2D Grounding to 3D World Coordinates

A critical challenge in UAV navigation is lifting 2D semantic detections into the 3D operational space. Mere 2D bounding boxes are insufficient for aerial control, which requires precise depth information to execute safe approach maneuvers. Upon acquiring the high-confidence 2D target coordinates $\mathbf{p}_{2D} = (x, y)$ from the MLLM, we perform a geometric lifting operation. We first retrieve the corresponding depth value $d = D_t(x, y)$ from the synchronized depth map D_t .

Leveraging the pinhole camera model, we back-project the

2D pixel coordinates (in homogeneous form) into the UAV’s instantaneous camera coordinate frame. This yields the relative 3D position of the target, denoted as \mathbf{G}_{cam} :

$$\mathbf{G}_{cam} = [X_c \ Y_c \ Z_c] = d \cdot K^{-1} \cdot [x \ y \ 1], \quad (4)$$

where $K \in \mathbb{R}^{3 \times 3}$ is the calibrated camera intrinsic matrix. However, \mathbf{G}_{cam} is defined in the local camera coordinate system. To establish a globally consistent navigation goal, we must transform this relative vector into the fixed world frame using the UAV’s kinematic chain. Let $T_{IC} = \{R_{IC}, t_{IC}\}$ denote the extrinsic transformation from the camera frame to the UAV’s body (IMU) frame. Given the UAV’s instantaneous 6-DoF pose $T_t = \{R_t, t_t\}$ mapping the body frame to the world frame, we derive the final 3D world coordinate \mathbf{G}_{world} as:

$$\mathbf{G}_{world} = R_t \cdot (R_{IC} \cdot \mathbf{G}_{cam} + t_{IC}) + t_t, \quad (5)$$

where R_{IC} and t_{IC} are obtained via offline hand-eye calibration. By maintaining the target in the global frame, the system achieves robustness against camera motion blur or temporary target loss, as \mathbf{G}_{world} serves as a persistent anchor for the navigation module.

4.3. 3D Point Cloud Mapping and Path Planning

This module ensures flight safety via explicit 3D geometry, operating independently of the VLM loop.

4.3.1. PROBABILISTIC OBSTACLE MAPPING

We construct a local map M using raw points \mathcal{P}_t^{lidar} from the onboard LiDAR. To ensure global consistency, points are transformed from the sensor frame to the world frame via:

$$\mathbf{p}_{world} = R_t \cdot (R_{ext} \cdot \mathbf{p}_l + \mathbf{t}_{ext}) + \mathbf{t}_t, \quad (6)$$

where $\mathbf{p}_l \in \mathcal{P}_t^{lidar}$ is the raw point, R_{ext} , \mathbf{t}_{ext} denote the sensor-to-body extrinsics, and R_t , \mathbf{t}_t represent the UAV's real-time pose. The resulting global set \mathcal{P}_t^{world} updates a sliding-window ring buffer map M for efficient collision queries.

4.3.2. TRAJECTORY OPTIMIZATION

Given the target \mathbf{G}_{3D} , we utilize **Ego-Planner** for gradient-based trajectory generation. We parameterize the trajectory as a uniform B-spline $\Phi(t)$, strictly constrained within the convex hull of its control points $\{p_1, \dots, p_N\}$. The k -th order B-spline is defined as:

$$\Phi(t) = \sum_{i=0}^k p_{i+j} B_{i,k}(t - t_j). \quad (7)$$

We formulate trajectory generation as a non-linear optimization problem minimizing $J = \lambda_s J_s + \lambda_c J_c + \lambda_d J_d$. To prioritize safety while ensuring smooth motion, we configure the optimization weights as $\lambda_s = 1.0$, $\lambda_c = 10.0$, and $\lambda_d = 1.0$, balancing smoothness, safety, and feasibility:

1) Smoothness (J_s): Minimizes the jerk \mathbf{A}_i (derivative of acceleration) at the i -th control point to reduce oscillation:

$$J_s = \sum_{i=1}^{N-1} |\mathbf{A}_i|_2^2. \quad (8)$$

2) Collision Avoidance (J_c): Penalizes control points when the distance to the nearest obstacle $d(p_i)$ falls below a safety threshold d_{safe} . To ensure the gradient remains smooth for optimization, we define the differentiable penalty function $F(\cdot)$ as a cubic barrier:

$$J_c = \sum_{i=1}^{N_c} F(d(p_i)), \quad \text{where} \quad (9)$$

$$F(d) = \begin{cases} 0 & \text{if } d \geq d_{safe} \\ (d_{safe} - d)^3 & \text{if } d < d_{safe} \end{cases}$$

where d_{safe} represents the collision clearance margin (set to 0.5m in our experiments).

3) Dynamical Feasibility (J_d): Enforces kinematic constraints so velocity v_i and acceleration a_i do not exceed physical limits. In our implementation, we set $v_{max} = 4.0$ m/s and $a_{max} = 3.0$ m/s² to support agile flight:

$$J_d = \sum_{i=1}^N \left(\max(0, |v_i|^2 - v_{max}^2)^2 + \max(0, |a_i|^2 - a_{max}^2)^2 \right). \quad (10)$$

Finally, we employ a receding horizon strategy. The optimizer continuously replans using the current state as a warm start whenever the map updates or the MLLM provides a new semantic target.

5. Experiment

5.1. Experimental Setup

5.1.1. SIMULATION ENVIRONMENTS

We utilize Unreal Engine 4 (UE4) and AirSim to establish a high-fidelity simulation. This combination replicates complex environmental dynamics (e.g., lighting, fog) and realistic vehicle physics, ensuring the synthesized data aligns with real-world distributions.

5.1.2. REAL-WORLD PLATFORM IMPLEMENTATION

We construct a custom quadrotor to validate real-world performance (details in Appendix C).

5.1.3. DATASETS

Our evaluation strategy encompasses standard benchmarks and a custom in-the-wild dataset:

Public Benchmarks (Simulation): We employ the **AerialVLN** and **OpenFly** datasets, generated within AirSim. These benchmarks contain 24 distinct urban and suburban maps paired with over 14,000 human-annotated navigation instructions. The instructions vary in linguistic complexity, ranging from explicit directional commands to ambiguous landmark descriptions. The average trajectory length corresponding to the navigation instructions is set to 200 meters.

Real-World Dataset: To evaluate generalization capabilities within unstructured physical environments, we curate a custom dataset spanning multiple campus and park scenarios. This collection encompasses diverse flight conditions, including narrow corridors and areas with dense vegetation. The dataset comprises 800 navigation instructions, with an average flight trajectory length of 50 meters.

5.1.4. EVALUATION METRICS

Adhering to standard protocols in UAV-based VLN research, we employ the following metrics for evaluation. To ensure robustness, the performance for each navigation instruction is calculated as the average over 20 independent trials.

Success Rate (SR): The ratio of navigation episodes where the UAV terminates within a threshold distance ($d_{th} = 5m$) of the ground-truth target coordinates.

Navigation Error (NE): The Euclidean distance between the agent's final position and the target destination, averaged across all episodes (in meters).

Average Execution Time (Time): The mean duration required to complete a successful navigation task, a proxy for computational efficiency and path optimality (in seconds).

5.1.5. BASELINES

We compare Fly0 against two categories of state-of-the-art approaches:

End-to-End Learning Methods: We select **OpenFly** (Gao et al., 2025), **AerialVLN** (Liu et al., 2023), **OpenUAV** (Wang et al., 2024), and **UAV-Flow** (Wang et al., 2025). These models employ deep neural networks to map visual inputs directly to control actions. They serve as a baseline for measuring the benefits of our modular architecture over black-box policies.

Zero-Shot Agent-Based Methods: We include **NAVGP** (Zhou et al., 2024), **STMR** (Gao et al., 2024), **CityNav-Agent** (Liu et al., 2024), and **SPF** (Hu et al., 2025). Similar to our method, these approaches leverage pre-trained LLMs or VLMs for reasoning but differ in their grounding mechanisms and planning strategies. Comparison with these methods highlights the advantages of our explicit 3D goal projection and gradient-based planning.

5.2. Results and Analysis

To systematically validate the effectiveness of the Fly0 framework and verify our claims regarding the “paradigm misalignment” in existing approaches, we structure our analysis around three core research questions:

RQ1 (Precision and Efficacy): Does decoupling semantic grounding from motion control effectively resolve the *Granularity Mismatch*, leading to higher navigation success rates and lower errors?

RQ2 (Robustness and Generalization): Can the explicit 3D geometric representation mitigate visual domain shifts and *Fragile Context Maintenance*, thereby ensuring superior robustness compared to **End-to-End and MLLM-based baselines**?

RQ3 (Efficiency): Does the modular architecture successfully address the *High Inference Latency* bottleneck inherent in MLLM-based controllers?

The quantitative results corresponding to these questions are summarized in Table 1. The detailed experimental flow is shown in Figure 3.

5.2.1. ANALYSIS OF RQ1: ADDRESSING GRANULARITY MISMATCH

Decoupling leads to superior precision. As highlighted in our Introduction, mapping sparse linguistic tokens directly to dense control signals often results in suboptimal trajectories. The results on the AerialVLN and OpenFly datasets strongly support our hypothesis that decoupling these tasks yields superior performance.

Fly0 achieves a SR of **70.43%** and **64.67%** on the two

simulation datasets, respectively, surpassing the strongest Zero-Shot baseline (SPF) by a margin of over **20%**. More critically, our method demonstrates a drastic reduction in NE. For instance, on AerialVLN, Fly0 reduces the error to **27.19m**, compared to **39.57m** for SPF and **67.78m** for the end-to-end OpenFly model.

We attribute this precision to the “Specialization” of modules. By offloading the “how to move” task to the gradient-based Ego-Planner, Fly0 ensures smooth, continuous geometric progression, solving the *Granularity Mismatch*. In contrast, methods like NAVGP and CityNavAgent, which force the LLM to function as a low-level controller, suffer from high NE ($> 59m$) because LLMs lack geometric intuition to output precise metric instructions.

In contrast, Fly0 maintains a robust SR of **62.86%** in the real-world dataset. This validates that our explicit 3D spatial representation serves as a stable anchor against visual perturbations. Once the MLLM grounds the target and the depth module projects it into 3D space (\mathbf{G}_{world}), the navigation becomes a geometric problem solved by LiDAR, which is invariant to lighting or seasonal changes. This effectively mitigates the *Fragile Context Maintenance* issue, as the agent does not need to continuously re-interpret the visual scene for every control frame, thereby reducing the risk of tracking loss due to occlusion.

5.2.2. ANALYSIS OF RQ2: ROBUSTNESS VIA GEOMETRIC EXPLICIT GROUNDING

Explicit 3D geometry ensures robustness against both visual gaps and context loss. As detailed in Table 1, Fly0 demonstrates superior generalization, particularly in the Real-World dataset (SR 62.86%), significantly outperforming both categories of baselines. This robustness stems from two distinct mechanisms tailored to the weaknesses of each baseline group:

(1) Mitigating Visual Domain Gaps (vs. End-to-End Models): End-to-End methods (e.g., OpenUAV) suffer a catastrophic performance drop (SR $\sim 20\% \rightarrow 13\%$) when transferring from simulation to reality. These “black-box” models tend to overfit to synthetic textures and lighting. Fly0 overcomes this by relying on LiDAR-based geometric planning. Once the target is semantically identified, the navigation process relies on point clouds, which are invariant to lighting conditions or texture variations. This ensures that the physical execution remains stable even when the visual appearance of the environment changes drastically.

(2) Mitigating Fragile Context and Hallucination (vs. Zero-Shot MLLM Agents): A critical failure mode for MLLM-as-Controller methods (e.g., NAVGP, CityNav-Agent) is the loss of temporal context. As observed in their high Navigation Error ($> 60m$), these agents struggle to

Table 1. Comparison results across different datasets. All baseline methods are configured with the MLLMs specified in their official implementations. Our approach utilizes Qwen2.5VL-32B.

Method	AerialVLN dataset			OpenFly dataset			Real-world dataset			
	SR \uparrow	NE \downarrow	Time \downarrow	SR \uparrow	NE \downarrow	Time \downarrow	SR \uparrow	NE \downarrow	Time \downarrow	
End-to-End	OpenUAV	20.41	63.04	53.19	17.81	74.63	64.16	13.19	27.39	20.72
	UAV-Flow	36.47	57.31	49.73	32.14	69.51	55.17	27.46	23.61	19.04
	AerialVLN	7.28	90.20	50.67	6.71	94.63	52.91	3.95	49.37	26.73
	OpenFly	37.72	67.78	45.31	33.61	64.08	50.72	29.08	25.60	18.36
Zero Shot	NAVGPT	34.04	59.41	113.61	29.28	61.57	117.48	26.31	33.87	39.47
	STMR	30.15	63.82	97.62	27.43	66.54	103.64	22.61	37.09	34.03
	CityNavAgent	28.97	66.34	126.74	25.33	70.24	131.75	22.17	38.71	42.39
	SPF	46.72	39.57	87.94	42.94	46.57	90.25	35.07	20.48	36.76
	Fly0(Ours)	70.43	27.19	63.09	64.67	29.47	64.81	62.86	13.76	22.03

maintain a consistent trajectory. When a target exits the field-of-view (FOV) due to UAV rotation or occlusion, pure VLM agents often “hallucinate” incorrect actions or stop prematurely because they lack a persistent spatial memory. Fly0 addresses this via Object Permanence. By projecting the 2D target into a global 3D coordinate (G_{world}), our system decouples navigation from continuous visual contact. Even if the target is occluded or leaves the camera frame during complex maneuvers, the explicit 3D goal remains fixed in the global map. This solves the *Fragile Context Maintenance* issue, allowing the UAV to navigate to the destination with a “memory” of the target’s location, rather than reacting solely to the instantaneous visual frame.

5.2.3. ANALYSIS OF RQ3: BALANCING EFFICIENCY AND LATENCY

Modular design mitigates high inference latency. The *High Inference Latency* of auto-regressive MLLMs is a major bottleneck for real-time flight. As shown in Table 1, “MLLM-as-Controller” methods (NAVGPT, CityNavAgent) incur prohibitive execution times ($> 113s$), as they require querying the heavy model at every decision step.

Fly0 optimizes the balance between reasoning capability and execution speed. It achieves an average completion time of **63.09 s**, performing nearly **2 \times faster** than competing zero-shot agents. Although Fly0 incurs a marginal latency overhead compared to reactive end-to-end models, this trade-off is justified as safety takes precedence over raw speed in aerial navigation. This efficiency results from our event-triggered strategy where the MLLM is queried solely for high-level goal grounding, while the lightweight Ego-Planner handles the 50 Hz control loop. These results confirm that utilizing the MLLM as a reasoning engine rather than a motion controller is critical for safe deployment on resource-constrained UAV platforms.

5.2.4. FAILURE CASE ANALYSIS

Despite the general robustness of Fly0, real-world testing reveals two specific limitations. First, semantic ambiguity occurs in environments with high object repetition. Under-specified instructions, such as selecting a specific tree in a dense forest, can cause the MLLM to erroneously ground the command to a similar but incorrect object. Second, depth-induced projection errors arise at the semantic-geometric interface. While the visual recognition of targets like distant structures or thin wires remains accurate, errors in depth estimation during 2D-to-3D projection can result in imprecise coordinate generation, leading the drone to undershoot or overshoot its target.

5.3. Ablation Study

Table 2. Ablation experiments for each component.

Method	AerialVLN dataset		
	SR \uparrow	NE \downarrow	Time \downarrow
Fly0 (wo. DI)	56.47	34.89	61.74
Fly0 (wo. TO)	61.33	32.41	58.76
Fly0 (wo. DI+TO)	41.82	47.03	54.75
Fly0	70.43	27.19	63.09

We conducted a comprehensive ablation study to evaluate the individual contributions of key components within the Fly0 framework. Results are shown in Table 2. First, we examined the Depth Image (DI) acquisition module. While our standard implementation utilizes sensor-based depth in both simulation and real-world settings, the ablated variant relies on MLLM-based depth estimation, following the methodology adopted by SPF. Experimental results demonstrate a significant decline in SR upon removing explicit depth acquisition. This degradation is attributed to the inherent inaccuracy of MLLM distance estimation, which introduces substantial deviations during the 2D-to-3D coordinate

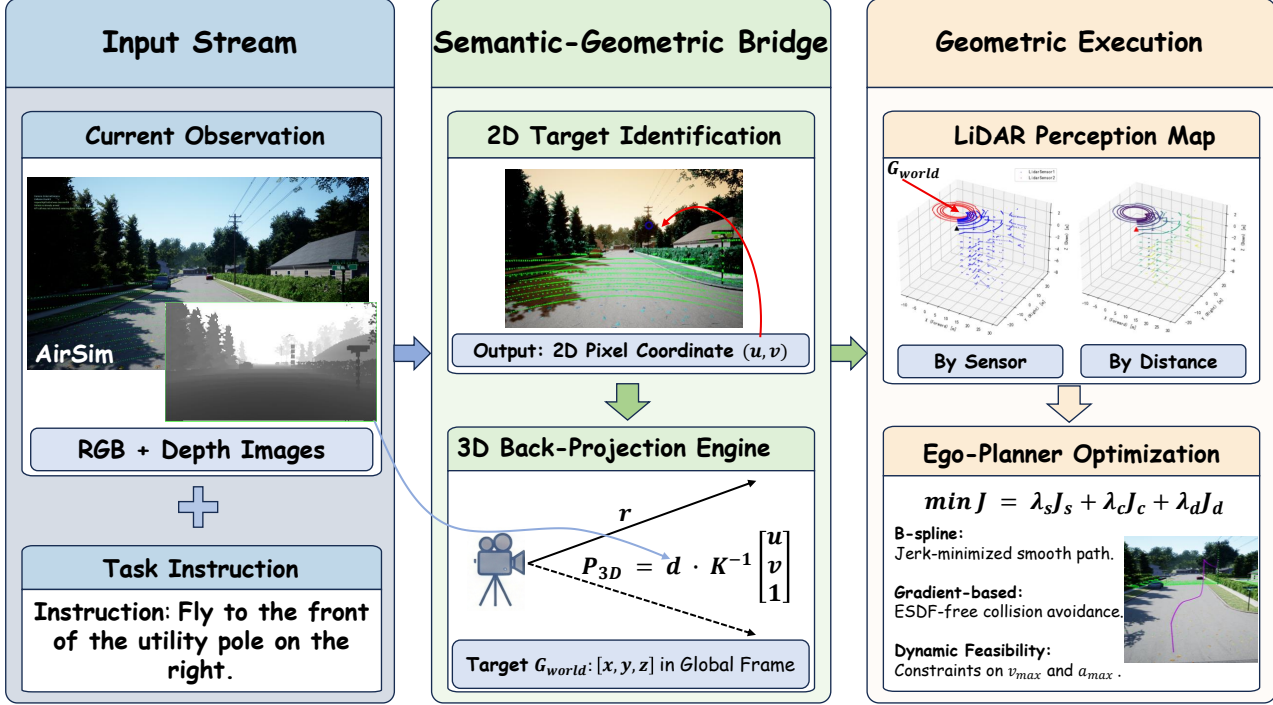


Figure 3. The execution pipeline from visual perception to trajectory optimization. First, the **Input Stream** combines RGB-D images and instructions to locate the target in the image frame. Next, the **Back-Projection Engine** maps this 2D point to the 3D world frame via the pinhole camera model. Finally, based on the projected 3D target and local LiDAR sensing, the **Ego-Planner** optimizes the flight path by solving a gradient-based problem to ensure collision-free and kinematically feasible motion.

projection. Such errors are particularly exacerbated in long-range navigation scenarios. Subsequently, we investigated the Trajectory Optimization (TO) component (Ego-Planner). In the absence of this module, the MLLM assumes responsibility for both path generation and obstacle avoidance. The results indicate that without real-time geometric planning, the system suffers a notable reduction in success rates due to collision vulnerability. Furthermore, the simultaneous removal of both components leads to a precipitous drop in overall navigation performance.

Table 3. Dependency testing for MLLM.

Method	AerialVLAN dataset		
	SR \uparrow	NE \downarrow	Time \downarrow
GPT 5	70.53	27.31	67.43
Gemini 3 Pro	70.66	26.94	68.37
Claude 3.7 Sonnet	70.51	27.35	65.94
DeepSeek VL	70.37	27.64	67.15
Qwen2.5VL-32B	70.43	27.19	63.09

We further evaluated the sensitivity of Fly0 to different MLLM backbones, demonstrating robust compatibility across varying model scales. We attribute this flexibility to

the nature of the referring coordinate grounding task, which primarily demands precise semantic recognition rather than complex multi-step logical reasoning. Consequently, models with fewer parameters can achieve performance parity with top-tier closed-source large models. Empirically, our method using Qwen2.5VL-32B exhibits negligible difference in navigation Success Rates compared to the advanced Gemini 3 Pro. This finding is pivotal for real-world applications; while high-capacity models often rely on API calls with unpredictable network latency, smaller models enable efficient local deployment. This ensures the low-latency inference required for safe, real-time UAV navigation.

6. Conclusion

In this work, we identify the inherent limitations of deploying MLLMs as direct motion controllers for UAV navigation, specifically highlighting the conflict between semantic reasoning latency and the real-time demands of flight dynamics. We propose Fly0, a framework that harmonizes these conflicting requirements by decoupling the navigation pipeline into MLLM-based semantic grounding and explicit geometric planning. By leveraging the semantic generalization of MLLMs solely for goal identification and offloading execution to a robust local planner, Fly0 achieves superior performance and interpretability.

Impact Statement

This paper presents work whose goal is to advance the field of Machine Learning. There are many potential societal consequences of our work, none which we feel must be specifically highlighted here.

References

Anderson, P., Wu, Q., Teney, D., Bruce, J., Johnson, M., Sünderhauf, N., Reid, I., Gould, S., and Van Den Hengel, A. Vision-and-language navigation: Interpreting visually-grounded navigation instructions in real environments. In *Proceedings of the IEEE conference on computer vision and pattern recognition*, pp. 3674–3683, 2018.

Chen, K., Chen, J. K., Chuang, J., Vázquez, M., and Savarese, S. Topological planning with transformers for vision-and-language navigation. In *Proceedings of the IEEE/CVF Conference on Computer Vision and Pattern Recognition*, pp. 11276–11286, 2021.

Fried, D., Hu, R., Cirik, V., Rohrbach, A., Andreas, J., Morency, L.-P., Berg-Kirkpatrick, T., Saenko, K., Klein, D., and Darrell, T. Speaker-follower models for vision-and-language navigation. *Advances in neural information processing systems*, 31, 2018.

Gao, Y., Wang, Z., Jing, L., Wang, D., Li, X., and Zhao, B. Aerial vision-and-language navigation via semantic-topo-metric representation guided llm reasoning. *arXiv preprint arXiv:2410.08500*, 2024.

Gao, Y., Li, C., You, Z., Liu, J., Li, Z., Chen, P., Chen, Q., Tang, Z., Wang, L., Yang, P., et al. Openfly: A comprehensive platform for aerial vision-language navigation. *arXiv preprint arXiv:2502.18041*, 2025.

Georgakis, G., Schmeckpeper, K., Wanchoo, K., Dan, S., Miltsakaki, E., Roth, D., and Daniilidis, K. Cross-modal map learning for vision and language navigation. In *Proceedings of the IEEE/CVF conference on computer vision and pattern recognition*, pp. 15460–15470, 2022.

Hao, W., Li, C., Li, X., Carin, L., and Gao, J. Towards learning a generic agent for vision-and-language navigation via pre-training. In *Proceedings of the IEEE/CVF conference on computer vision and pattern recognition*, pp. 13137–13146, 2020.

Hong, Y., Wu, Q., Qi, Y., Rodriguez-Opazo, C., and Gould, S. Vln bert: A recurrent vision-and-language bert for navigation. In *Proceedings of the IEEE/CVF conference on Computer Vision and Pattern Recognition*, pp. 1643–1653, 2021.

Hu, C. Y., Lin, Y.-S., Lee, Y., Su, C.-H., Lee, J.-Y., Tsai, S.-R., Lin, C.-Y., Chen, K.-W., Ke, T.-W., and Liu, Y.-L. See, point, fly: A learning-free vlm framework for universal unmanned aerial navigation. In *Conference on Robot Learning*, pp. 4697–4708. PMLR, 2025.

Huang, C., Mees, O., Zeng, A., and Burgard, W. Visual language maps for robot navigation. *arXiv preprint arXiv:2210.05714*, 2022.

Liang, J., Huang, W., Xia, F., Xu, P., Hausman, K., Ichter, B., Florence, P., and Zeng, A. Code as policies: Language model programs for embodied control. *arXiv preprint arXiv:2209.07753*, 2022.

Liu, S., Zhang, H., Qi, Y., Wang, P., Zhang, Y., and Wu, Q. Aerialvln: Vision-and-language navigation for uavs. In *Proceedings of the IEEE/CVF International Conference on Computer Vision*, pp. 15384–15394, 2023.

Liu, Y., Yao, F., Yue, Y., Xu, G., Sun, X., and Fu, K. Nav-agent: Multi-scale urban street view fusion for uav embodied vision-and-language navigation. *arXiv preprint arXiv:2411.08579*, 2024.

Sautenkov, O., Yaqoot, Y., Lykov, A., Mustafa, M. A., Tadevosyan, G., Akhmetkazy, A., Cabrera, M. A., Martynov, M., Karaf, S., and Tsetserukou, D. Uav-vla: Vision-language-action system for large scale aerial mission generation. In *2025 20th ACM/IEEE International Conference on Human-Robot Interaction (HRI)*, pp. 1588–1592. IEEE, 2025.

Shah, D., Osiński, B., Levine, S., et al. Lm-nav: Robotic navigation with large pre-trained models of language, vision, and action. In *Conference on robot learning*, pp. 492–504. PMLR, 2023.

Wang, X., Huang, Q., Celikyilmaz, A., Gao, J., Shen, D., Wang, Y.-F., Wang, W. Y., and Zhang, L. Reinforced cross-modal matching and self-supervised imitation learning for vision-language navigation. In *Proceedings of the IEEE/CVF conference on computer vision and pattern recognition*, pp. 6629–6638, 2019.

Wang, X., Yang, D., Wang, Z., Kwan, H., Chen, J., Wu, W., Li, H., Liao, Y., and Liu, S. Towards realistic uav vision-language navigation: Platform, benchmark, and methodology. *arXiv preprint arXiv:2410.07087*, 2024.

Wang, X., Yang, D., Liao, Y., Zheng, W., Dai, B., Li, H., Liu, S., et al. Uav-flow colosseo: A real-world benchmark for flying-on-a-word uav imitation learning. *arXiv preprint arXiv:2505.15725*, 2025.

Xu, H., Hu, Y., Gao, C., Zhu, Z., Zhao, Y., Li, Y., and Yin, Q. Geonav: Empowering mllms with explicit geospatial reasoning abilities for language-goal aerial navigation. *arXiv preprint arXiv:2504.09587*, 2025.

Zhang, W., Gao, C., Yu, S., Peng, R., Zhao, B., Zhang, Q., Cui, J., Chen, X., and Li, Y. Citynavagent: Aerial vision-and-language navigation with hierarchical semantic planning and global memory. *arXiv preprint arXiv:2505.05622*, 2025.

Zhao, Y., Xu, K., Zhu, Z., Hu, Y., Zheng, Z., Chen, Y., Ji, Y., Gao, C., Li, Y., and Huang, J. Cityeqa: A hierarchical llm agent on embodied question answering benchmark in city space. *arXiv preprint arXiv:2502.12532*, 2025.

Zhou, G., Hong, Y., and Wu, Q. Navgpt: Explicit reasoning in vision-and-language navigation with large language models. In *Proceedings of the AAAI Conference on Artificial Intelligence*, volume 38, pp. 7641–7649, 2024.

Zhou, X., Wang, Z., Ye, H., Xu, C., and Gao, F. Ego-planner: An esdf-free gradient-based local planner for quadrotors. *IEEE Robotics and Automation Letters*, 6(2):478–485, 2020.

Zhu, F., Zhu, Y., Chang, X., and Liang, X. Vision-language navigation with self-supervised auxiliary reasoning tasks. In *Proceedings of the IEEE/CVF conference on computer vision and pattern recognition*, pp. 10012–10022, 2020.

A. Prompt Design for MLLM

Figure 4 presents the complete prompt template utilized to guide the MLLM in translating visual inputs and navigation instructions into precise 2D coordinates.

Please locate the destination specified by the user within the image based on the user's complete instruction. The image dimensions are 720x480 pixels, with the origin (0,0) at the top-left corner.

Please note the following when understanding the user's instruction:

The user may include directional information (e.g., "front-left", "right side", "front", etc.), which indicates the target's relative position in the image;

The user may include the target type (e.g., "car", "ball", "door", etc.), which is the object to be detected;

You must combine the directional information and target type to locate the destination that best matches the user's description.

Please handle the request according to the following scenarios:

1. If the target described by the user exists in the image, please return the center pixel coordinates (X,Y) of only the single most relevant target (the most prominent one or the one closest to the user's description).

The format must be "(X,Y)".

2. If the target described by the user does not exist in the image, please return "(0,0)".

Return only the coordinates; do not include any other content.

Figure 4. The full text of the prompt used to guide the MLLM. It instructs the model to locate the destination specified in the user's command within the 2D image frame and return its pixel coordinates, handling cases of both target existence and absence.

B. Navigation Trajectory Results

Figures 5 and 6 offer a more comprehensive analysis of the experimental results.

C. Details of Experimental Setup

To ensure reproducibility and facilitate further research, we provide detailed specifications of our physical aerial platform and the computational infrastructure used in the real-world experiments.

C.1. UAV Platform and Hardware Configuration

We utilized a custom-built quadrotor platform, the TTF-400LIVO-RTK, designed for autonomous navigation in complex unstructured environments. The platform is built upon a resilient, collision-tolerant carbon fiber frame with a diagonal wheelbase of 320mm. The core hardware components include:

Flight Controller: A Pixhawk 6C Mini running the PX4 autopilot firmware, equipped with an STM32H743 processor for stable flight attitude control.

Onboard Computer: An NVIDIA Jetson Orin NX (16GB) serves as the edge computing unit. It features an 8-core Arm Cortex-A78AE CPU and a 1024-core NVIDIA Ampere architecture GPU, providing up to 100 TOPS of AI performance. This unit is responsible for sensor data processing, visual transmission, and real-time trajectory generation.

Perception Sensors: 1) **LiDAR:** A Livox Mid-360 hybrid solid-state LiDAR provides omnidirectional 3D point clouds (360° horizontal FOV) at a rate of 200,000 points/sec for obstacle mapping. 2) **Vision:** An Stereolabs ZED 2i camera is mounted front-facing to capture visual semantics and depth information for the grounding module.

Positioning: For outdoor experiments, we utilized a high-precision RTK GNSS module (OEM-982) with 4G connectivity to provide centimeter-level ground truth for evaluation.

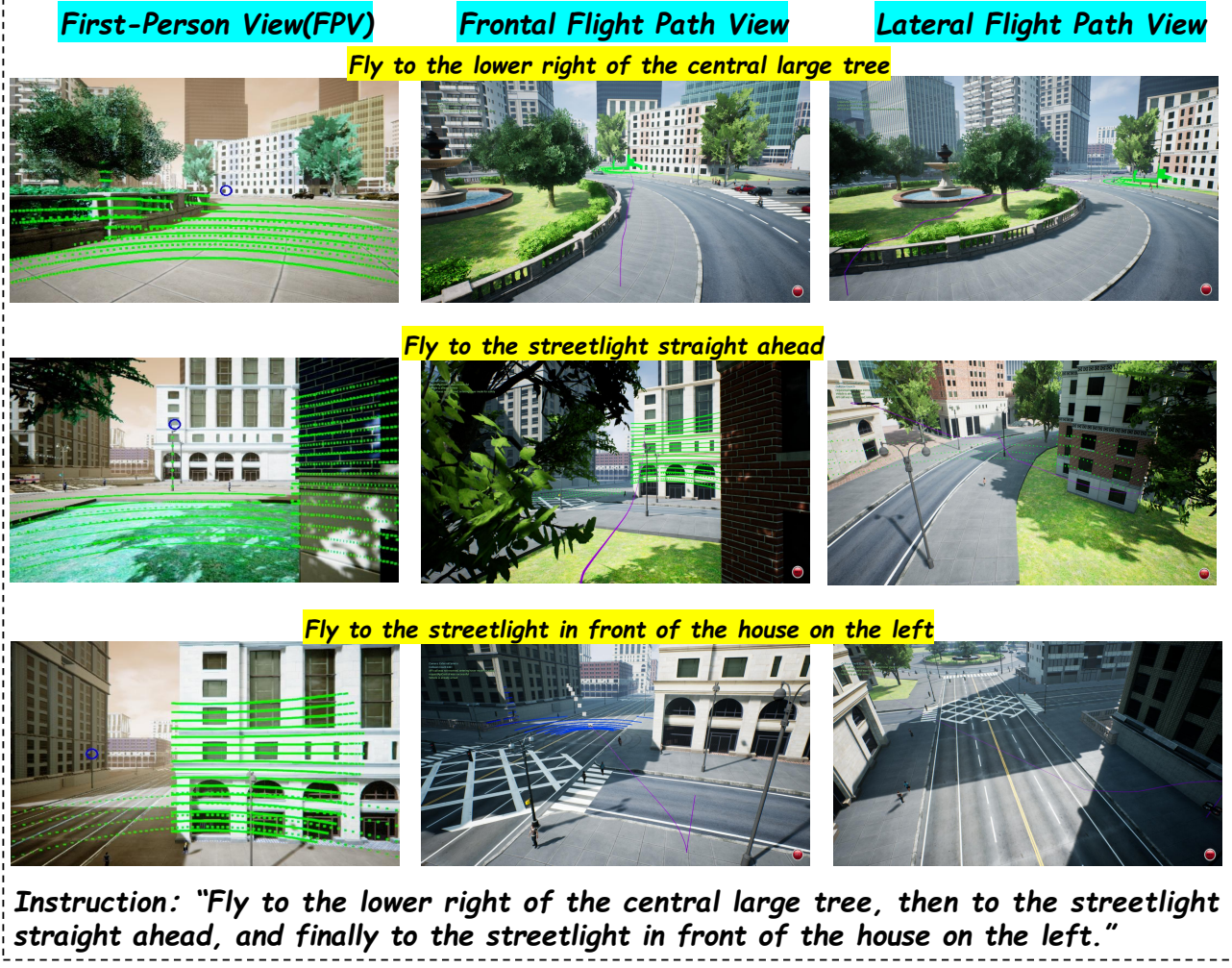


Figure 5. Qualitative visualization of a sequential navigation task in a complex urban environment. The UAV executes a multi-step composite instruction (bottom) sequentially. The three rows correspond to the three sub-tasks: approaching the tree, navigating to the streetlight, and reaching the final destination. The columns display the onboard First-Person View (FPV) with LiDAR perception, followed by Frontal and Lateral views of the generated collision-free trajectory (purple curve).

C.2. Computational Architecture and Deployment

Our system adopts a hybrid Cloud-Edge Collaborative Architecture to balance the computational demands of large-scale semantic reasoning with the real-time requirements of flight control:

Server-Side Semantic Reasoning (Cloud): The computationally intensive Multimodal Large Language Model (MLLM) is deployed on a remote high-performance server cluster equipped with $4 \times$ NVIDIA A800 GPUs. During operation, the UAV transmits compressed first-person view (FPV) images to the server via a low-latency API. The server executes the 2D Semantic Goal Grounding module (as described in Sec. 4.1) and returns the pixel coordinates of the target to the UAV.

Onboard Geometric Planning (Edge): The NVIDIA Jetson Orin NX onboard the UAV handles all latency-critical tasks locally using the ROS Noetic environment.



Figure 6. Extensive qualitative evaluation across diverse simulation environments. The figure presents six additional independent trials ranging from urban streets to parks and island terrains. Each row depicts the successful execution of a long-horizon composite instruction (displayed at the bottom). These results demonstrate the robustness of Fly0 in handling heterogeneous scene topologies and its capability to ground fine-grained spatial constraints (e.g., “rise above”, “cross over”, “hover over”) into precise physical trajectories.